GEOPHYSICS, VOL. 55, NO. 10 (OCTOBER 1990); P. 1366–1379, 8 FIGS., 4 TABLES.

An accurate and efficient scheme for wave propagation in linear viscoelastic media

H. Tal-Ezer*, J. M. Carcione‡, and D. Kosloff§

ABSTRACT

The problem of wave propagation in a linear viscoelastic medium can be described mathematically as an exponential evolution operator of the form $e^{\mathbf{M}t}$ acting on a vector representing the initial conditions, where $\mathbf{M}$ is a spatial operator matrix and t is the time variable. Techniques like finite difference, for instance, are based on a Taylor expansion of this evolution operator. We propose an optimal polynomial approximation of $e^{\mathbf{M}t}$ based on the powerful method of interpolation in the complex plane, in a domain which includes the eigenvalues of the matrix $\mathbf{M}$.

The new time-integration technique is implemented to solve the isotropic viscoacoustic equation of motion. The algorithm is tested for the problem of wave propagation in a homogeneous medium and compared with second-order temporal differencing and the spectral Chebychev method. The algorithm solves efficiently, and with machine accuracy, the problem of seismic wave propagation with a dissipation mechanism in the sonic band, a characteristic of sedimentary rocks. The computational effort in forward modeling based on the new technique is half compared to that of temporal differencing when two-digit precision is required. Accuracy is very important, particularly for propagating distances of several wavelengths, since the anelastic effects should not be confused with nonphysical phenomena, such as numerical dispersion in time-stepping methods. Finally, we compute the seismic response to a single shot in a realistic geologic model which includes a gas-cap zone in an anticlinal fold. The results clearly show the importance of the attenuation and dispersion effects for an appropriate interpretation of the seismic data. In particular, the gas-cap response (a bright spot) suffers significant variations in amplitude, phase, and arrival time compared to the purely acoustic case.

INTRODUCTION

The problem of wave propagation in anelastic media has practical value in many fields: geophysics, ocean acoustics, applied mechanics, and physics of materials, etc. (Borcherdt, 1982; Szilard, 1982; Ferry, 1970). Linear viscoelasticity provides a general framework to describe the anelastic effects in wave propagation, i.e., the conversion of part of the energy into heat and the dispersion of the wave field Fourier components with increasing time. The main difficulty in implementing the linear viscoelastic and anisotropic constitutive relation in the equation of motion is the presence of convolutional integrals. This problem was solved by assuming a complex viscoelastic modulus which is a rational function in the frequency domain. Within this context, the time-domain equation of motion can be written in differential form by introducing additional variables into the formulation (Day and Minster, 1984; Emmerich and Korn, 1987; Carcione et al., 1988a).

Spectral methods have recently become a very useful tool for the solution of time-dependent differential equations. Generally, a spectral method is applied to calculate the spatial derivatives, and a finite-difference approach is used to march the solution in time. This results in an imbalanced scheme with infinite spatial accuracy but only second-order temporal accuracy. Carcione et al. (1988a,b) used the Fourier method to compute the spatial derivative terms and a spectral time-integration technique to solve the isotropic

Manuscript received by the Editor July 18, 1988; revised manuscript received April 16, 1990.
*School of Mathematical Science, Tel-Aviv University, Tel-Aviv 69918 Israel.
‡Observatorio Geofisico Sperimentale, P.O. Box 2011, 34016 Trieste, Italy, and Geophysical Institute, Hamburg University, 2000 Hamburg 13, West Germany.
§Dept. of Geophysics and Planetary Sciences, Tel-Aviv University, Tel-Aviv 69978, and Geophysical Institute, Hamburg University, 2000 Hamburg 13, West Germany.

viscoacoustic and viscoelastic equations of motion. We refer to this technique as the spectral Chebychev method (see also Tal-Ezer et al., 1987). However, this method as originally designed to solve wave propagation in elastic media, although very accurate, is, in general, inefficient in terms of computer time for viscoelastic wave propagation problems. On the other hand, by using second-order temporal differencing, it is possible to have efficiency but not high accuracy, and accuracy is very important in anelastic propagation where the numerical dispersion could be taken as physical dispersion.

We propose a new time-integration method specially designed to deal with wave propagation in linear viscoelastic and anisotropic media. As with the Chebychev method, the equations governing wave motion are recast as a single first-order matricial differential equation in time. After spatial discretization, a coupled system of ordinary differential equations is obtained. The formal solution is the exponential evolution operator $e^{\underline{\mathbf{M}}t}$ (where $\underline{\mathbf{M}}$ is an operator matrix containing the spatial derivatives and t is the time variable) acting on the initial condition vector (homogeneous case), or a similar operator acting on the source spatial distribution vector (inhomogeneous case). The technique can be applied to a number of methods for spatial derivation, including the finite-difference, finite-element, and Fourier methods.

The spectral Chebychev method consists of a Chebychev polynomial expansion of the evolution operator whose region of convergence (in the Fourier method approximation) is the imaginary axis of the complex wavenumber plane. In anelastic propagation, however, the eigenvalues of the matrix $\underline{\mathbf{M}}$ lie on a T-shaped domain D which includes the negative real axis and the imaginary axis; hence, a more appropriate expansion is required. The new approach is based on a polynomial interpolation of the exponential function in the complex domain D, in a set of points known to have maximal properties. This set of points is found through a conformal mapping between the unit disc and the domain of the eigenvalues D. In this way, the interpolating polynomial is "almost best" (Tal-Ezer, 1989).

The first section presents the governing equation of motion. To illustrate the properties of the method, we choose the isotropic viscoacoustic wave propagation problem, analyzed in detail in the following sections. Then we develop and justify the polynomial approximation of the evolution operator in the homogeneous and inhomogeneous cases, and describe the forward modeling algorithm. The scheme is then compared to second-order temporal differencing, the spectral Chebychev method, and known analytical solutions. Finally, we show how to solve a realistic problem which computes the seismic response to a single shot of a complex structure containing a hydrocarbon cap in an anticlinal fold, a typical trap in exploration geophysics. Viscoacoustic and acoustic seismograms and snapshots are compared.

EQUATION OF MOTION

In n-dimensional media the linearized equation of momentum conservation is

$$\rho\ddot{\mathbf{u}} = \nabla \cdot \underline{\boldsymbol{\Sigma}} + \mathbf{f}, \tag{1}$$

where $\mathbf{u}(\mathbf{x}, t)$ is the displacement field, $\underline{\boldsymbol{\Sigma}}(\mathbf{x}, t)$ is the stress tensor, $\mathbf{f}(\mathbf{x}, t)$ represents the body forces, $\rho(\mathbf{x})$ is the density, and $\mathbf{x}$ is the position vector. A dot above a variable denotes time differentiation. For a linear viscoelastic and anisotropic solid, the most general relation between the components of the stress tensor σ_{ij}, and the components of the strain tensor $\varepsilon_{k\ell}$, is given by Boltzmann's superposition principle:

$$\sigma_{ij} = \psi_{ijk\ell} * \dot{\varepsilon}_{k\ell}, \qquad k,\ell = 1, \ldots, n, \tag{2}$$

where $\psi_{ijk\ell}(\mathbf{x}, t)$ is a fourth-rank tensorial relaxation function. The asterisk denotes time convolution, and repeated indices imply summation. Wave motion is described by substitution of equation (2) into the equation of motion, equation (1). However, implementation of Boltzmann's superposition principle in the time domain is not straightforward due to the presence of convolutional kernels in equation (2). This problem was solved by Carcione et al (1988a,c) for the isotropic viscoacoustic case and Carcione et al. (1988b) for the viscoelastic case. To avoid the time convolutions in equation (2), it is necessary to introduce additional variables called memory variables. The numerical algorithm requires that the equation of motion be recast as a first-order differential equation in time as

$$\dot{\mathbf{E}} = \underline{\mathbf{M}}\mathbf{E} + \mathbf{S}, \tag{3}$$

where $\mathbf{E}$ is a vector whose components are the unknown variables, $\underline{\mathbf{M}}$ is an operator matrix containing the spatial derivatives, and $\mathbf{S}$ is the body force vector. To illustrate the nature of the problem, we next consider the simplest case: wave motion in an isotropic linear viscoacoustic medium.

VISCOACOUSTIC WAVE PROPAGATION

The constitutive relation for n-dimensional viscoacoustic media is expressed by

$$p = -\dot{e} * \psi, \tag{4}$$

where $p(\mathbf{x}, t)$ is the pressure, $e(\mathbf{x}, t)$ is the dilatation, and $\psi(\mathbf{x}, t)$ is the relaxation function given by

$$\psi(t) = M_R \left[1 - \sum_{\ell=1}^{L} \left(1 - \frac{\tau_{\varepsilon\ell}}{\tau_{\sigma\ell}} \right) e^{-t/\tau_{\sigma\ell}} \right] H(t), \tag{5}$$

in which $\tau_{\sigma\ell}(\mathbf{x})$ and $\tau_{\varepsilon\ell}(\mathbf{x})$ denote material relaxation times for the ℓth mechanism, L is the number of relaxation mechanisms, $M_R(\mathbf{x})$ is the relaxed modulus, and $H(t)$ is the step function (see Carcione et al., 1988a).

The equation of motion is obtained by taking divergence in the equation of momentum conservation (1):

$$-\mathbf{D}\rho = \ddot{e} + s, \tag{6}$$

where $s(\mathbf{x}, t)$ is a source term given by the divergence of the body forces divided by the density, and $\mathbf{D}$ is a spatial derivative operator defined by

$$\mathbf{D} = \frac{\partial}{\partial x_i} \left[\frac{1}{\rho} \frac{\partial}{\partial x_i} \right], \qquad i = 1, \ldots, n. \tag{7}$$

After introducing the memory variables, it is possible to write the equation of motion for the viscoacoustic solid in the form of equation (3), where

$$\mathbf{E}^T = [e, \dot{e}, e_{1\ell}, \ldots, e_{1L}], \tag{8}$$

with $e_{1\ell}$, $\ell = 1, \ldots, L$ being the memory variables,

$$\mathbf{S}^T = [0, s, 0, \ldots, 0] \tag{9}$$

is the source term, and

$$\underline{\mathbf{M}} = \begin{bmatrix} 0 & 1 & 0 & 0 & \cdots & 0 \\ \mathbf{D}M_u & 0 & \mathbf{D} & \mathbf{D} & \cdots & \mathbf{D} \\ \phi_1 & 0 & -1/\tau_{\sigma 1} & 0 & \cdots & 0 \\ \phi_2 & 0 & 0 & -1/\tau_{\sigma 2} & \cdots & 0 \\ \vdots & \vdots & \vdots & \vdots & \vdots & \vdots \\ \phi_L & 0 & 0 & 0 & \cdots & -1/\tau_{\sigma L} \end{bmatrix} \tag{10}$$

the spatial matrix, where $M_u(\mathbf{x}) \equiv \psi(\mathbf{x}, 0)$ is called the unrelaxed modulus, and

$$\phi_\ell = \frac{M_R}{\tau_{\sigma\ell}}\left(1 - \frac{\tau_{\varepsilon\ell}}{\tau_{\sigma\ell}}\right), \qquad \ell = 1, \ldots, L \tag{11}$$

is the response function at $t = 0$, corresponding to the ℓth mechanism.

Spatial discretization of the equation of motion

The spatial derivative terms in equation (3) are calculated with the Fourier method, which consists of a discretization in space and computation of the spatial derivatives by means of the fast Fourier transform (Kosloff and Baysal, 1982).

Considering an n-dimensional medium, system (3) becomes a coupled system of

$$(L+2)N \equiv (L+2)\prod_{i=1}^{n} N_i,$$

ordinary differential equations in the unknown variables at the grid points, where N_i, $i = 1, \ldots, n$ denote the number of grid points in the x_i direction.

The semidiscrete representation of the system to be solved can be written in compact notation as

$$\mathbf{E}_N = \underline{\mathbf{M}}_N \mathbf{E}_N + \mathbf{S}_N, \tag{12}$$

subject to the initial condition

$$\mathbf{E}_N(t-0) = \mathbf{E}_N^0, \tag{13}$$

where $\mathbf{E}_N$ and $\mathbf{S}_N$ are vectors of dimension $(L+2)N$, and $\underline{\mathbf{M}}_N$ is a $(L+2)N \cdot (L+2)N$ matrix. The solution of equation (12) subject to equation (13) is formally given by

$$\mathbf{E}_N = e^{t\underline{\mathbf{M}}_N} + \int_0^t e^{\tau\underline{\mathbf{M}}_N}\mathbf{S}_N(t-\tau)\,d\tau. \tag{14}$$

The quantity $e^{t\underline{\mathbf{M}}_N}$ is called the evolution operator. Most frequently, an explicit or implicit finite-difference scheme is used to march the solution in time (Day and Minster, 1984; Emmerich and Korn, 1987). These algorithms are based on a Taylor expansion of the evolution operator.

Eigenvalues of the matrix $\underline{\mathbf{M}}$

Considering constant material properties and a zero source term, a plane-wave solution to equation (3) is assumed of the form

$$\mathbf{E} = \mathbf{E}_0 e^{i(\omega_c t - \boldsymbol{\kappa}\cdot\mathbf{x})}, \tag{15}$$

where $\omega_c = \omega + i\omega_I$ is the complex angular frequency and $\boldsymbol{\kappa}$ is the real wavenumber. Substitution of equation (15) in equation (3) yields

$$i\omega_c\mathbf{E} = \begin{bmatrix} 0 & 1 & 0 & 0 & \cdots & 0 \\ -\dfrac{M_u\kappa^2}{\rho} & 0 & -\dfrac{\kappa^2}{\rho} & -\dfrac{\kappa^2}{\rho} & \cdots & -\dfrac{\kappa^2}{\rho} \\ \phi_1 & 0 & -1/\tau_{\sigma 1} & 0 & \cdots & 0 \\ \phi_2 & 0 & 0 & -1/\tau_{\sigma 2} & \cdots & 0 \\ \vdots & \vdots & \vdots & \vdots & \vdots & \vdots \\ \phi_L & 0 & 0 & 0 & \cdots & -1/\tau_{\sigma L} \end{bmatrix}$$

$$\mathbf{E} \equiv \hat{\underline{\mathbf{M}}}E. \tag{16}$$

Equation (16) is an eigenvalue equation for the eigenvalues $\lambda = i\omega_c$. The discretized characteristic equation corresponding to equation (16) is

$$|\hat{\underline{\mathbf{M}}}_N - \underline{\mathbf{I}}\lambda| = 0, \tag{17}$$

where $\underline{\mathbf{I}}$ is the identity matrix. The n-dimensional wavenumber is

$$\kappa^2(v_i) = \sum_{i=1}^{n} \kappa_i^2(v_i), \tag{18}$$

with

$$\kappa_i = \frac{2\pi v_i}{N_i DX_i}, \qquad v_i = -\frac{N_i}{2}, \ldots, \frac{N_i}{2}, \tag{19}$$

where DX_I is the grid spacing in the x_i direction. For instance, for $L = 1$ the characteristic equation results in

$$\left(\lambda_v + \frac{1}{\tau_\sigma}\right)[\lambda_v^2 + \omega_0^2(v)] - \lambda_v\omega_0^2(v)\left(\frac{\tau_\varepsilon}{\tau_\sigma} - 1\right) = 0, \tag{20}$$

where $\omega_0(v) = c_R\kappa(v)$, with $c_R = \sqrt{M_R/\rho}$, the relaxed velocity of the medium.

There are three solutions for each v in equation (20). When the attenuation is not too strong, we have $(\tau_\varepsilon/\tau_\sigma - 1) \ll 1$. Under this condition, one eigenvalue, say $\lambda_v^{(1)}$, is close to $-1/\tau_\sigma$, and the others $\lambda_v^{(2)}$ and $\lambda_v^{(3)}$ lie in the vicinity of $-i\omega_0(v)$ and $i\omega_0(v)$, respectively. The first eigenvalue corresponds to a static mode that attenuates with time, and the others correspond to propagating waves.

For instance, in the 1-D case, for $\tau_\varepsilon = 0.0016$ s, $\tau_\delta = 0.0015$ s, $c_R = 2000$ m/s, and $\kappa = \kappa(N/2) = \pi/DX$, $DX = 10$ m, the Nyquist (maximum) wavenumber, the eigenvalues are $\lambda^{(1)} = -645.73\ \mathrm{s}^{-1}$, $\lambda^{(2)} = (-10.46 + 638.33i)\ \mathrm{s}^{-1}$, and $\lambda^{(3)} = \bar{\lambda}^{(2)}$, where the bar denotes complex conjugate.

Figure 1 shows the eigenvalues of the matrix $\underline{\mathbf{M}}_N$ when

$N = 22$, (a) $\tau_\varepsilon = 0.0016$ s, $\tau_\sigma = 0.0015$ s, and (b) $\tau_\varepsilon = 0.0020$, $\tau_\sigma = 0.0015$ s. We refer to the complex plane of the eigenvalues as the z-plane. The eigenvalues corresponding to the Nyquist and zero wavenumbers are represented by the largest circles. The propagating modes lie near the imaginary axis and the static modes are clustered around $-1/\tau_\sigma$ which is the solution for $v = 0$.

Carcione et al. (1988c) show that the spatial quality factor for a viscoacoustic solid is given by

$$Q_e(\omega) = \frac{\text{Re}\,[M_c(\omega)]}{\text{Im}\,[M_c(\omega)]}, \tag{21}$$

where $M_c(\omega) = \tilde{\psi}(t)$ is the complex bulk modulus, and Re and Im denote real and imaginary parts, respectively; the tilde indicates time Fourier transform. The quality factor measures the degree of attenuation of the wave field. The lower Q_e, the stronger is the dissipation. When $L = 1$,

$$Q_e(\omega) = \frac{1 + \omega^2\tau_\varepsilon\tau_\sigma}{\omega(\tau_\varepsilon - \tau_\sigma)}. \tag{22}$$

This function has a minimum at $\omega_m = 1/\sqrt{\tau_\varepsilon\tau_\sigma}$. Substitution of the relaxation times in equation (22) results in a lower minimum for case (b). As shown in Figure 1, a lower Q_e implies a shift of the eigenvalues to the left of the imaginary axis.

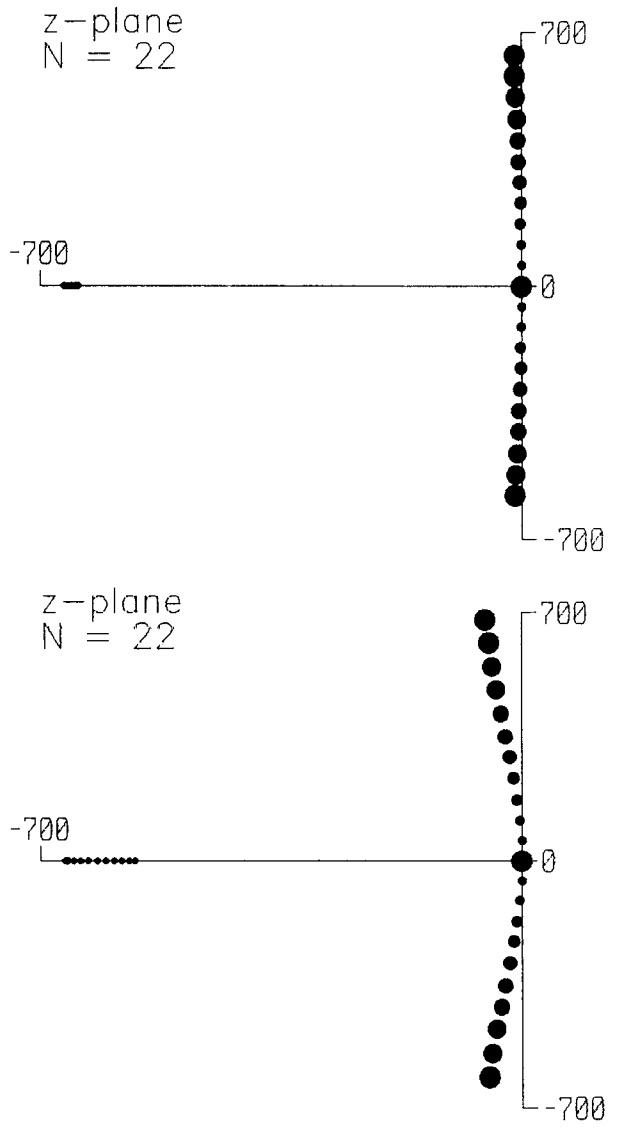

FIG. 1. Eigenvalues of the spatial matrix $\underline{\mathbf{M}}$, for $N = 22$, (a) $\tau_\varepsilon = 0.0016$ s, $\tau_\sigma = 0.0015$ s, and (b) $\tau_\varepsilon = 0.0020$ s, $\tau_\sigma = 0.0015$ s. The relaxed velocity is $c_R = 2000$ m/s. The propagating modes lie near the imaginary axis and the static modes are clustered around $-1/\tau_\sigma$, which is the solution corresponding to zero wavenumber.

THE ALGORITHM

A polynomial interpolation of the evolution operator is obtained in Appendix A. The interpolation is done in a set of points which have maximal properties of convergence; this set of points is found through a conformal mapping between the unit disc (u-space) and the domain of the eigenvalues of $\underline{\mathbf{M}}_N$(z-space). The polynomial in Newton form is

$$P_m(z) = a_0 + a_1(z - z_0) + a_2(z - z_0)(z - z_1) + \cdots + a_m(z - z_0)\cdots(z - z_{m-1}), \tag{23}$$

where z_j and a_j, $j = 0, \ldots, m - 1$ are the interpolating points and divided differences, respectively, and m is the order.

The problem is to calculate $\mathbf{E}_N(t)$ in equation (14) by using the polynomial approximation, i.e.,

$$\mathbf{E}_N(t) = P_m(t, \underline{\mathbf{M}}_N)\mathbf{V}_N. \tag{24}$$

In the homogeneous case (zero source term) the polynomial is

$$P_m(t, \underline{\mathbf{M}}_N) \equiv P_m^{(H)}(t, \underline{\mathbf{M}}_N) \simeq e^{t\underline{\mathbf{M}}_N}, \tag{25}$$

with

$$\mathbf{V}_N = \mathbf{E}_N^0. \tag{26}$$

In the inhomogeneous case we have

$$P_m(t, \underline{\mathbf{M}}_N) \equiv P_m^{(I)}(t, \underline{\mathbf{M}}_N) \simeq \int_0^t e^{\tau\underline{\mathbf{M}}_N} h(t - \tau)\, d\tau, \tag{27}$$

with

$$\mathbf{V}_N = \mathbf{A}_N \tag{28}$$

the source spatial distribution, and $h(t)$ the time function, such that $\mathbf{S} = \mathbf{A}h$.

The numerical method used to solve the viscoelastic equation of motion in previous works (Carcione et al., 1988a, b,c) is a particular case of the present method (Tal-Ezer, 1989). In the spectral Chebychev method, the polynomials used to approximate the evolution operator are scaled, modified Chebychev polynomials. Thus, an efficient algorithm which uses the three-term recurrence relation was implemented. However, this scheme is efficient when the domain D of the eigenvalues of $\underline{\mathbf{M}}_N$ is on the imaginary axis or close to it. To solve the viscoelastic equation of motion, the parameter B, defined in equation (A-3), should be chosen large enough that the resulting region of convergence includes the nonpropagating modes situated on the negative

real axis. In this case, accuracy is assured if the number terms of the Chebychev series satisfy $m_1 > Bt$. When the domain D is on the negative real axis (e.g., the diffusion equation), the polynomials are scaled Chebychev (Tal-Ezer, 1985). In this case, the number of terms is constrained to $m_2 > 2.5\ (At)^{0.6}$, where A is given by equation (A-3). The present algorithm is found to be accurate when the degree of the polynomial is $m > \max\ (m_1, m_2)$.

The arrangement of the interpolating points plays a significant role in reducing the roundoff errors. The points z_j, $j = 0, \ldots, m-1$ have to be ordered such that the interpolating points in u-space, $u_j, j = 0, \ldots, m-1$, are equally distributed on the circle of radius δ, where δ is the logarithmic capacity of the conformal mapping equation (A-4). The program given in Appendix A generates the interpolating points according to this requirement. It yields $u_0 = \delta(z_0 = 0)$, $u_1 = -\delta(z_1 = -A)$, and u_i, $i = 2, \ldots, k-1$, as illustrated in Figure 2, where $k = 10$ ($m = 20$) is displayed. The angle between adjacent points is π/k. The ordering is indicated by the size of the circles with the smallest one corresponding to u_0. The right side of Figure 2 shows the interpolating points z_i. The points of the lower u-plane, $\bar{u}_i$, map to the complex conjugate of the lower z-plane points. When Re $[u_i] > 0$, the points are purely imaginary, and when Re $[u_i] < 0$, the points lie on the negative real axis.

The calculation of $\mathbf{E}_N(t)$ can be carried out in real arithmetic even if z_j and a_j in equation (23) are complex numbers, since the m interpolating points $z_j, j = 0, \ldots, m-1$ can be arranged as $z_0, z_1, z_2, \bar{z}_2, \ldots, z_k, \bar{z}_k$, 2k points, where z_0 and z_1 are real numbers. Tal-Ezer (1989) proved that if $f(\bar{z}) = \overline{f(z)}$ [$f(z)$ defined in equations (A-1a) and (A-1b) satisfies this property], and the interpolating points are defined as before, the interpolating polynomial has real coefficients. Consequently, the polynomial can be expressed as (Tal-Ezer, 1989),

$$P_{2k-1}(z) = a_0 + a_1(z - z_0) + (z - z_0)(z - z_1) \sum_{i=1}^{k-1} S_i(z) R_i(z), \tag{29}$$

where

$$S_i(z) = \text{Re}\ [a_{2i}] + \text{Re}[a_{2i+1}]\{z - \text{Re}\ [z_{i+1}]\}, \tag{30a}$$

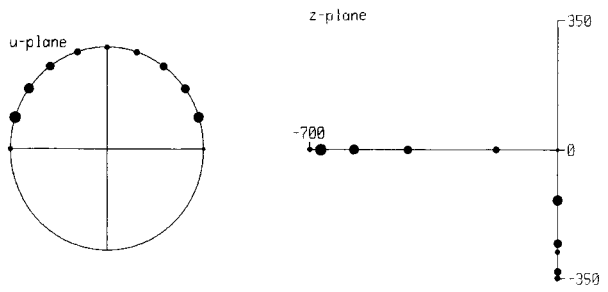

FIG. 2. Interpolating points in z-space obtained by a conformal mapping $z = \chi(u)$ from u-space ($m = 20$). The points of the lower u-plane, $\bar{u}_i$, map to the complex conjugates of the lower z-plane points.

and

$$R_1(z) = 1, \quad R_i(z) = \prod_{j=2}^{i} (z - z_j)(z - \bar{z}_j), \quad i = 2, \ldots, k-1. \tag{30b}$$

Based on equation (29), the solution is computed by

$$\mathbf{E}_N(t) = P_{2k-1}(t, \underline{\mathbf{M}}_N)\mathbf{V}_N, \tag{31}$$

using the following algorithm:

$$\mathbf{E}_N = [a_0 \underline{\mathbf{I}} + a_1(\underline{\mathbf{M}}_N - z_0 \underline{\mathbf{I}})]\mathbf{V}_N, \tag{32a}$$

$$\mathbf{R}_N = (\underline{\mathbf{M}}_N - z_0 \mathbf{I})(\underline{\mathbf{M}}_N - z_1 \underline{\mathbf{I}})\mathbf{V}_N, \tag{32b}$$

the first step, and for $i = 1, \ldots, k-1$:

$$\mathbf{Q}_N = \{\underline{\mathbf{M}}_N - \text{Re}\ [z_{i+1}]\underline{\mathbf{I}}\}\mathbf{R}_N, \tag{32c}$$

$$\mathbf{E}_N = \mathbf{E}_N + \text{Re}\ [a_{2i}]\mathbf{R}_N + \text{Re}\ [a_{2i+1}]\mathbf{Q}_N, \tag{32d}$$

$$\mathbf{R}_N = \{\underline{\mathbf{M}}_N - \text{Re}\ [z_{i+1}]\underline{\mathbf{I}}\}\mathbf{Q}_N + \text{Im}^2[z_{i+1}]\mathbf{R}_N. \tag{32e}$$

The algorithm requires three vectors, $\mathbf{Q}_N$ and $\mathbf{R}_N$ as auxiliary arrays, and $\mathbf{E}_N$ to accumulate the solution.

The forward modeling algorithm

With the method just described, we can construct a forward modeling algorithm. For seismic modeling, we start with zero initial conditions. The first time interval should be greater than the duration of the source time function, say t_0. The solution is obtained as

$$\mathbf{E}_N(t_0) = \left[\int_0^{t_0} e^{\tau \underline{\mathbf{M}}_N} h(t_0 - \tau)\, d\tau\right]\mathbf{A}_N \simeq P_{2k-1}^{(I)}(t_0, \underline{\mathbf{M}}_N)\mathbf{A}_N. \tag{33}$$

The solution can be propagated in time again by considering $\mathbf{E}_N(t_0)$ as an initial condition using the homogeneous solution

$$\mathbf{E}_N(t) = e^{t\underline{\mathbf{M}}_N}\mathbf{E}_N(t_0) \simeq P_{2k-1}^{(H)}(t, \underline{\mathbf{M}}_N)\mathbf{E}_N(t_0). \tag{34}$$

The calculation of seismograms at a given point of the medium does not require significant extra effort, since only additional divided differences, which contain the time dependence, need be generated.

Since the Fourier method considers the discretized variables on the grid as periodic functions, absorbing boundaries are implemented to prevent wraparound, the phenomenon where a pulse which exits the grid on one side reenters it on the opposite side. To eliminate this effect, we use a method developed by Kosloff and Kosloff (1986), based on a gradual elimination of amplitudes in a strip surrounding the numerical mesh. More details can be found in Tal-Ezer et al. (1987), where the method is modified slightly to increase its efficiency.

EXAMPLES

We first test the new algorithm for the 1-D viscoacoustic problem to illustrate its resolution properties and efficiency in terms of computer time compared with temporal differ-

encing and the spectral Chebychev method. Second, comparison with a known analytical solution in a 2-D medium is performed. Finally, we compute the response of a realistic geologic model to a single shot. We refer to the spectral Chebychev technique as method 1 and the present algorithm as method 2.

One-dimensional wave propagation

Comparison with the spectral Chebychev method.—Let us consider the initial value problem in a 1-D medium with constant velocity and density. This problem was solved in Carcione et al. (1988a), where the solution is obtained by first solving the acoustic wave equation and then applying the correspondence principle. Assuming an initial condition of the form

$$e(x, 0) = e^{-\eta K_0^2 x^2} \cos(\varepsilon \pi K_0 x), \tag{35}$$

with K_0 the cutoff wavenumber, and ε and η constants, the viscoelastic solution is given by

$$e_v(x, t) = \mathbf{F}^{-1}[\tilde{e}_v(x, \omega)], \tag{36}$$

where

$$\tilde{e}_v(x, \omega) = \pi \sqrt{\frac{\pi}{\eta}} \frac{1}{k_0 v(\omega)} \cos\left[\omega \frac{x}{v(\omega)}\right] \times \left\{\exp\left[-\frac{\pi^2}{\eta}\left(\frac{\varepsilon}{2} - \frac{\omega}{k_0 v(\omega)}\right)^2\right] + \exp\left[-\frac{\pi^2}{\eta}\left(\frac{\varepsilon}{2} + \frac{\omega}{k_0 v(\omega)}\right)^2\right]\right\}, \tag{37}$$

with $k_0 = 2\pi K_0$ and $v(\omega)$ the complex velocity given by

$$v(\omega) = \sqrt{\frac{M_c(\omega)}{\rho}}. \tag{38}$$

The operator $\mathbf{F}^{-1}$ performs the inverse time Fourier transform. The relaxed bulk modulus is $M_R = 8$ GPa, and the density $\rho = 2000$ kg/m^3, which give a relaxed velocity $c_R = 2000$ m/s. The relaxation times are defined in Table 1. They give an almost constant quality factor $Q_e \simeq 100$ in the seismic exploration band. Figures 3a and 3b show the quality factor and phase velocity versus frequency. The phase velocity is calculated as $c(\omega) = \omega/\mathrm{Re}\,[k_c]$, where $k_c = \omega/v(\omega)$ is the complex wavenumber. Assuming $K_0 = 1/40$ m^{-1}, $\eta = 0.5$, and $\varepsilon = 1.$, the analytical solution at $x_0 = 400$ m and $t_0 = 0.2$ s is

$$2e_v(x_0, t_0) = 0.7528533138. \tag{39}$$

Assuming that the relaxed velocity is the acoustic velocity, the solution corresponds to the main peak of the signal with amplitude $2e(x_0, t_0) = 1$, in the acoustic limit (i.e., $Q_e \to \infty$, or $\tau_{\varepsilon\ell} \to \tau_{\sigma\ell}$, $\ell = 1, \ldots, L$).

The numerical solution is computed by using a number of grid points $N = 198$ and a grid spacing $DX = 10$ m. This sampling is sufficient to assure that the error comes solely from the time integration method. Table 2 illustrates the

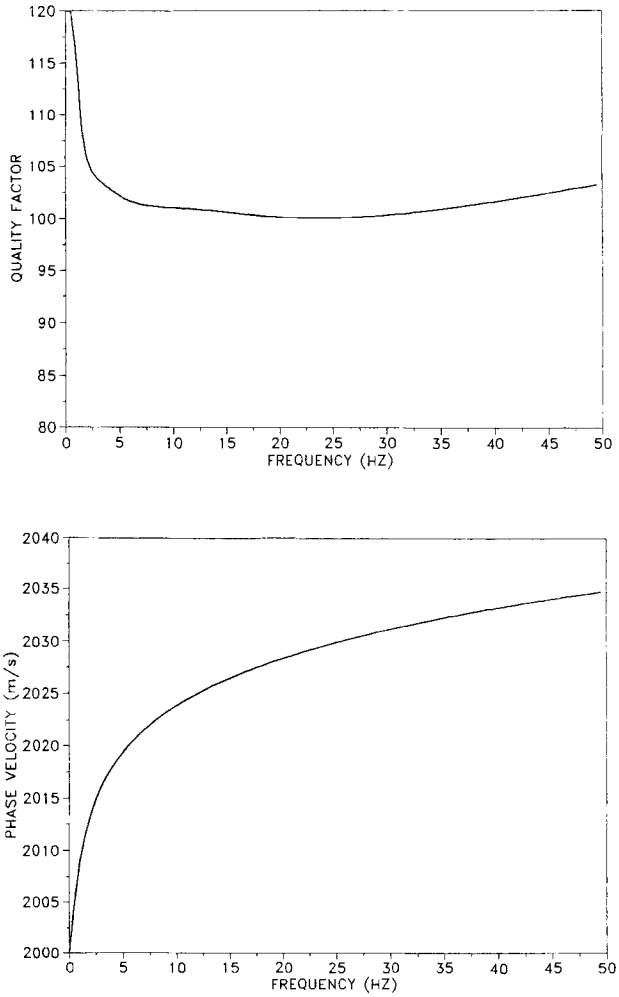

FIG. 3. (a) Spatial quality factor versus frequency, (b) phase velocity versus frequency. The medium is defined by a relaxed bulk modulus $M_R = 8$ GPa, a density $\rho = 2000$ kg/m^3, and the five sets of relaxation times given in Table 1. They give an almost constant Q_e value in the seismic exploration band.

Table 1. Relaxation times.

l	τ_{ε_l}	τ_{σ_l}
1	0.3196389	0.3169863
2	0.0850242	0.0842641
3	0.0226019	0.0224143
4	0.0060121	0.0059584
5	0.0016009	0.0015823

Table 2. Resolution properties.

Method 1 m_1	Method 2 m	Error
275	140	$<10^{-1}$
285	150	$<10^{-3}$
290	160	$<10^{-4}$
300	166	$<10^{-6}$
320	185	$<10^{-10}$

resolution properties of methods 1 and 2, with m_1 the number of terms of the Chebychev series and m the degree of the interpolating polynomial. These quantities are equal to the number of operations to be performed with the matrix $\underline{\mathbf{M}}$, which represents the main computational effort since it requires the evaluation of the spatial derivatives. For method 1, a value of $B = 1334\ s^{-1}$ is necessary to obtain convergence. Method 2 requires $A = 633\ s^{-1}$ and $B = 628\ s^{-1}$. The result for $m = 185$ shows that while the minimum value required to have an acceptable resolution (two digits) is $m = 150$, increasing m by only 23 percent is enough to match the analytical solution by up to ten digits. Method 1 requires a higher B value and therefore more number of terms to obtain the same accuracy. As mentioned above, this condition insures the inclusion of the non-propagating modes in the region of convergence.

It has been proven experimentally that in sedimentary rocks there is a minimum in the quality factor in the sonic band around 2 kHz. The dissipation mechanism has been modeled by Murphy et al. (1986). The theory assumes the existence of narrow cracks between the surfaces of the grains in contact. As the grains oscillate under the presence of a perturbation, the pore fluid is squeezed out of, and sucked back into, the cracks. The energy is dissipated by viscous shearing. To simulate these conditions, we take $\tau_\varepsilon = 8 \times 10^{-5}$ s and $\tau_\sigma = 7 \times 10^{-5}$ s. The quality factor and velocity dispersion are represented in Figures 4a and 4b, respectively. The relaxation times yield a quality factor $Q_e \simeq 600$ in the seismic exploration band and practically no velocity dispersion. With the same conditions as the previous example, the analytical solution is

$$2e_v(x_0, t_0) = 0.9733393369. \tag{40}$$

For t_0 of the order of milliseconds, method 1 solves the problem but it is not useful for wave propagation times used in seismic prospecting since the method is sensitive to the quantity t_0/τ_0, which in this case exceeds the dynamic range of the computer (see Carcione et al., 1988a).

Method 2 requires $A = 14\ 286\ s^{-1}$ and $B = 628\ s^{-1}$. To match the analytical solution with an error less than 10^{-10}, a polynomial of degree $m = 610$ is necessary. The degree is greater than in the previous example, a consequence of smaller relaxation times which increase the value of the eigenvalues corresponding to the nonpropagating modes.

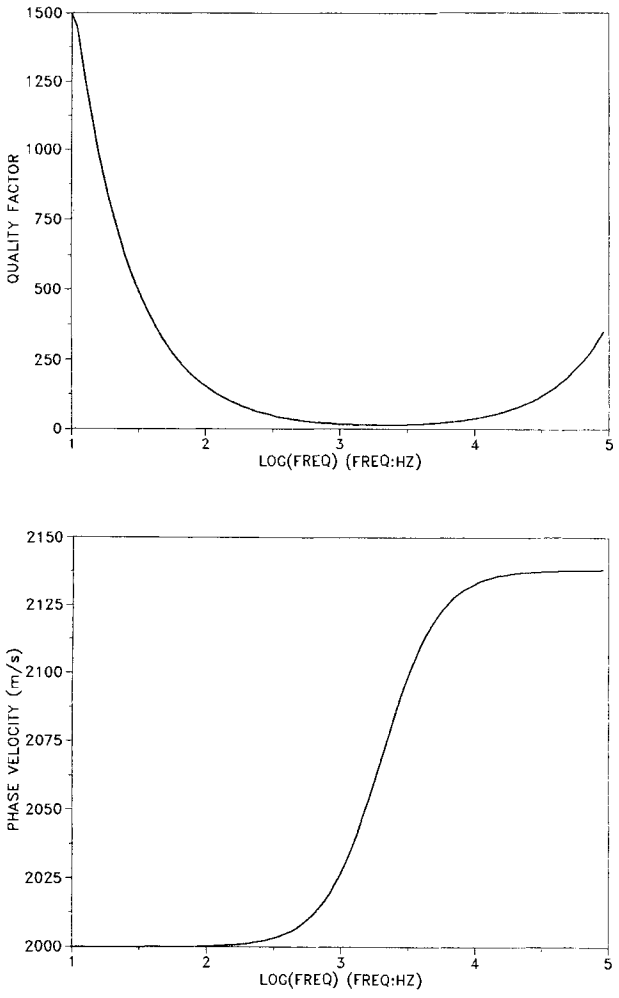

FIG. 4. (a) Spatial quality factor versus frequency, (b) phase velocity versus frequency. The medium is defined by a relaxed bulk modulus $M_R = 8$ GPa, a density $\rho = 2000$ kg/m^3, and $\tau_\varepsilon = 8 \times 10^{-5}$ s, and $\tau_\sigma = 7 \times 10^{-5}$ s. These relaxation times give a minimum in the quality factor in the sonic band, a typical phenomenon in sedimentary rocks.

Comparison with second-order temporal differencing.—It is instructive to compare the new time integration technique with the established second-order temporal differencing since this method is widely used in forward and inverse modeling, and particularly for wave propagation in anelastic media. The spatial derivatives are computed by using the Fourier method and, therefore, the numerical dispersion is due only to the temporal approximation.

Let us consider the 1-D viscoacoustic equation of motion with L relaxation mechanisms. We require L memory variables $e_{1\ell}$, $\ell = 1, \ldots, L$, and we obtain from equations (3), (8), (9), and (10)

$$\ddot{e} = \mathbf{D}\left[M_u e + \sum_{\ell=1}^{L} e_{1\ell} \right], \tag{41a}$$

and

$$\dot{e}_{1\ell} = e\phi_\ell - \frac{e_{1\ell}}{\tau_{\sigma\ell}}, \qquad \ell = 1, \ldots, L \tag{41b}$$

where

$$M_u = M_R\left[1 - \sum_{\ell=1}^{L} \left(1 - \frac{\tau_{\varepsilon\ell}}{\tau_{\sigma\ell}} \right) \right], \tag{42}$$

and ϕ_ℓ is given by equation (11). Denoting the time step by Δt, the time variable is discretized by $t = q\Delta t$. Following the approach of Emmerich and Korn (1987), we establish the second-order scheme

$$\ddot{e}^q = \frac{e^{q+1} - 2e^q + e^{q-1}}{\Delta t^2}, \tag{43a}$$

$$e_{1\ell}^q = \frac{e_{1\ell}^{q+1/2} + e_{1\ell}^{q-1/2}}{2}, \tag{43b}$$

and

$$\dot{e}_{1\ell}^{q} = \frac{e_{1\ell}^{q+1/2} - e_{1\ell}^{q-1/2}}{\Delta t}. \tag{43c}$$

Substitution of these expressions in equations (41a) and (41b) yields

$$e_{1\ell}^{q+1/2} = A_\ell e^q + B_\ell e_{1\ell}^{q-1/2} \tag{44a}$$

and

$$e^{q+1} = \Delta t^2 \mathbf{D}\left[M_u e^q + \sum_{\ell=1}^{L} \frac{e_{1\ell}^{q+1/2} + e_{1\ell}^{q-1/2}}{2} \right] + 2e^q - e^{q-1}, \tag{44b}$$

with

$$A_\ell = \frac{2\tau_{\sigma\ell}\Delta t\phi_\ell}{2\tau_{\sigma\ell} + \Delta t}, \tag{45a}$$

and

$$B_\ell = \frac{2\tau_{\sigma\ell} - \Delta t}{2\tau_{\sigma\ell} + \Delta t}. \tag{45b}$$

Let us consider the problem of the previous section whose analytical solution is given by equation (39), but, in this case, in single precision arithmetic. The finite-difference problem requires initial conditions for the dilatation and its time derivative, or equivalently, the dilatation at $t = 0$ and at $t = \Delta t$. $e(\Delta t)$ is computed numerically by using a very small time step in order to obtain machine accuracy. An alternative approach is to compute it by means of the correspondence principle, which can be used to check the numerical solution. In Table 3, we compare our scheme to second-order temporal differencing. The first column represents the number of digits required to match the analytical solution. The CPU time corresponds to a Microvax computer. The time step is indicated for finite differencing and the degree of the polynomial for method 2. For two-digit precision, which we think is a necessary condition for computing wave fields in anelastic media, method 2 is almost two times faster than finite differencing. To obtain machine accuracy, the present technique does not require much additional CPU time, while finite differencing is completely impractical.

To illustrate the approximations introduced by finite differencing, in Appendix B we calculate the phase velocity dispersion in a 1-D medium with L relaxation mechanisms.

Table 3. Efficiency.

	Finite differences		Method 2	
Digits	dt (ms)	CPU time (s)	m	CPU time (s)
1	1.	36	170	37
2	0.5	68	172	38
3	0.2	167	174	38
4	0.1	330	176	38
5	0.01	3290	190	43

Two-dimensional wave propagation

Comparison to analytical time history.—The problem involves wave propagation in a homogeneous viscoacoustic medium. The calculations use a 132 × 132 grid with $DX = DZ = 20$ m the grid spacing. The source is a shifted zero phase wavelet defined by

$$h(t) = \exp\left[-\frac{1}{2} f_0^2 (t - t_c)^2 \cos \pi f_0 (t - t_c) \right], \tag{46}$$

with $t_c = 0.06$ s and a high cutoff frequency of $f_0 = 50$ Hz. The same material properties of the one-dimensional problem are used in this problem (relaxation times given in Table 1). The analytical solution is obtained by means of the correspondence principle. A detailed derivation can be found in Carcione et al. (1988a).

Figure 5 compares numerical and analytical time histories at a distance of 800 m of the source. It can be seen that the better agreement is obtained with method 2. Method 1 shows some discrepancies near the onset of the signal. It can be shown that this problem appears due to the presence of the smaller relaxation time which makes the quantity t_0/τ_σ approach the dynamic range of the computer.

Common-shot experiment.—In this example, we compute a common-shot seismogram of an inhomogeneous structure with a wide range of seismic velocities and quality factors. We show in detail how to handle this realistic problem. The geological model is represented in Figure 6. It is a typical hydrocarbon trap where the reservoir rock, a permeable sandstone, is saturated with gas in region 5 and with brine in region 6. The gas-cap zone and the brine-saturated sandstone are highly dissipative. The anticlinal fold is enclosed between impermeable shales represented by media 4 and 7. The material properties are indicated in Table 4 where the relaxed velocities are given. The quality factors were chosen such that they have constant value around the dominant

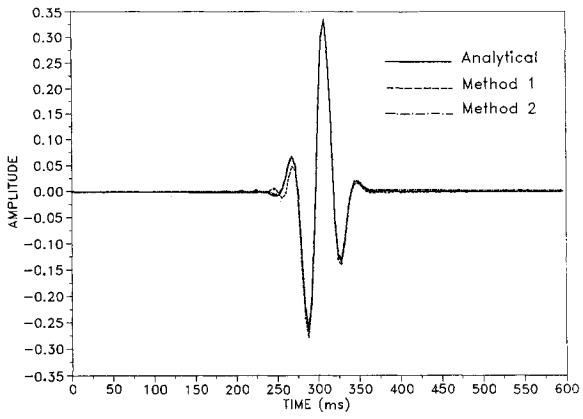

FIG. 5. Seismogram comparison between analytical and numerical solutions at a station located 800 m from the source. The source time function is given by equation (46). The medium is two-dimensional with the same material properties indicated in Figure 3.

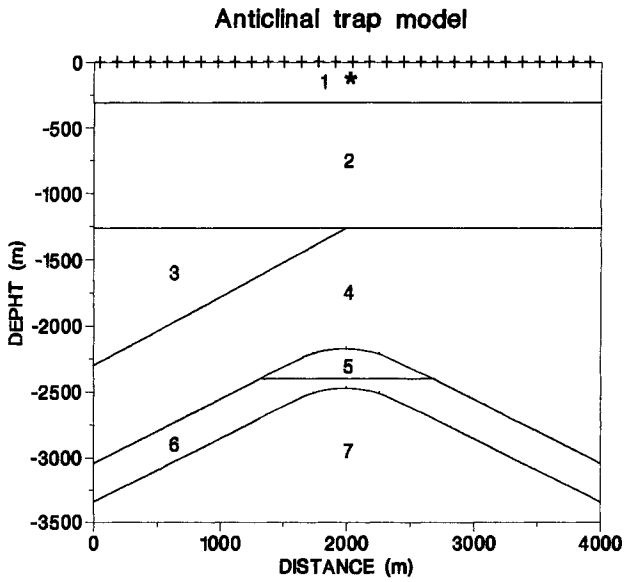

FIG. 6. Anticlinal trap model and configuration for the common-shot experiment. The numbers indicate the media whose properties are given in Table 4. * denotes the source and + the receivers.

frequency of the wavelet (30 Hz) which is given in equation (46). The source, represented by a star, is located in the weathering zone (medium 1) at a depth of 140 m, and the wave field is recorded by 168 geophones situated at the free surface. The calculations use a grid size of $N_x = 198$ and $N_z = 185$, with horizontal and vertical grid spacings of $DX = DZ = 20$ m. The free-surface condition was obtained by zero padding in the vertical direction to 308 grid points. This is equivalent to having the region of grid points between 186 and 308 in the vertical direction with zero velocity. To prevent wave-field wraparound, we use an absorbing region of 18 points surrounding the numerical mesh.

The anelastic properties in each region are obtained by using two sets of relaxation times, i.e., the modeling uses two memory variables, which together with the dilatation and its time derivative yield $N_v = 4$ unknown variables [see equation (8)]. Since the algorithm uses three vectors [see equations (32a–e)], total memory requirements are $3N_vN_xN_z$, which amounts to 0.44 megawords for the present model.

The numerical solution is propagated to 2 s with a first increment of $t_0 = 0.12$ s by using the inhomogeneous formulation and additional increments of 0.1 s with the homogeneous formulation. The parameters A and B can be estimated according to the eigenvalues of the matrix $\underline{\mathbf{M}}$ given by equation (17) and the criterion given by equation (A-3), i.e., to consider the highest eigenvalues. This procedure requires resolution of the eigenvalue problem. A simpler way is to consider the range of the eigenvalues for a homogeneous medium. For the Fourier method, this range is given by

$$A \simeq -\tau_\sigma^{-1}, \tag{47a}$$

and

$$B \simeq (\kappa_x^2 + \kappa_z^2)_{\max}^{1/2} c_R = \pi c_R (DX^{-2} + DZ^{-2})^{1/2}, \tag{47b}$$

with κ_x and κ_z denoting the real wavenumbers in x and z. In general, c_R should be taken as the highest velocity in the grid and τ_σ the minimum relaxation time. Since this is an approximation, an additional safety margin should generally be taken due to the heterogeneity of the medium and the absorbing boundary conditions. For the source time interval, for instance, the algorithm requires $A = 385\ \text{s}^{-1}$ and $B = 1732\ \text{s}^{-1}$ with a polynomial degree m = 374 according to the criterion $m > \max(m_1, m_2)$.

For comparison, the acoustic response of the model is also computed. The relaxed velocities given in Table 4 were taken as acoustic velocities. Note that the acoustic case is obtained by setting $\tau_{\varepsilon\ell} = \tau_{\sigma\ell}$, $\ell = 1, \ldots, L$. The seismic responses are shown in Figure 7, with (a) acoustic and (b) and (c) viscoacoustic. To display later events, the samples were multiplied by t^3. Figure 7c displays the same data given in (b) with an additional uniform gain (factor three). The source and the free surface combined act as a dipole source which produces the duplication of the reflected events with a period of approximately 0.1 s. For instance, the pinchout response at 1 s and the gas-cap response (a bright spot between 1.2 s and 1.5 s) appear in pairs with reversed polarity. The attenuation of the wave field is evident in Figure 7b, while the dispersion effects can be appreciated by comparing Figures 7a and 7c. For instance, the events

Table 4. Material properties.

Medium	c_R (m/s)	Q
1	2600	80
2	3200	100
3	4000	120
4	5200	250
5	3650	30
6	4300	60
7	6000	300

corresponding to the bottom of medium 2 (0.8 s) and the bright spot (1.3 s) arrive earlier in the viscoacoustic case. This is a consequence of taking the acoustic case in the low-frequency limit. This difference is relative, since the acoustic case could be chosen in the high-frequency limit, and then the opposite effect takes place. The bright-spot event is a combination of reflections from the upper and lower interfaces of the anticline and the gas-brine contact. Since these reflections are very close to each other, besides changes in arrival time, anelasticity also causes phase and amplitude variations which significantly alter the characteristics of the bright-spot response. In particular, the absorbing region appears to have performed well. No trace of wraparound is present at later times despite the gain function applied to the data. This fact is very important since the anelastic efffects should not be disturbed by nonphysical causes.

The energy dissipation can also be appreciated by comparing acoustic and viscoacoustic snapshots. They are represented in Figures 8a–8b at 0.72 s propagating time, and in Figures 8c–8d at 0.82 s propagating time. As can be seen, two wavefronts of reversed polarity travel close to each other, more attenuated in the viscoacoustic case. The representations include the absorbing region at the sides. The snapshots indicate that perturbations arising from the finite dimensions of the model practically do not exist.

CONCLUSIONS

Wave propagation in anelastic media is correctly described within the framework of the theory of linear viscoelasticity by assuming that the material rheology is represented by the general standard linear solid constitutive relation. This assumption introduces nonpropagating modes whose eigenvalues lie on the negative real axis of the complex wavenumber plane. Hence, the domain of the eigenvalues of the evolution operator, which in the elastic case is the imaginary axis, also includes the real negative axis. A convenient approximation of the evolution operator

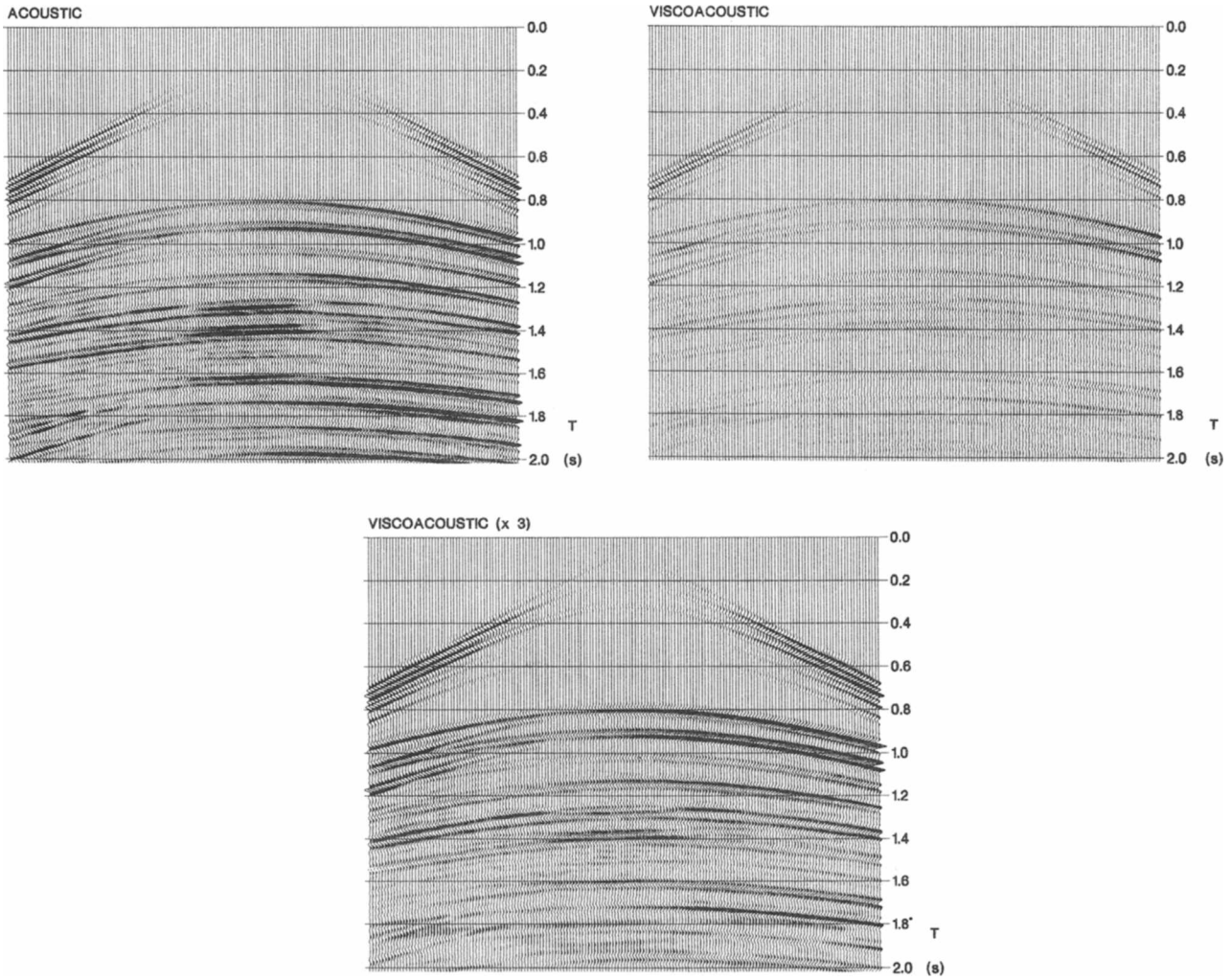

FIG. 7. Synthetic time sections corresponding to the anticlinal trap model, with (a) acoustic and (b) and (c) viscoacoustic. The data are displayed with a cubic gain in time. (c) is the same as (b) with an additional uniform gain (factor three). The source time function is given by equation (46).

is done by polynomial interpolation at optimal points of the domain of the eigenvalues.

The resulting algorithm is used to solve the isotropic viscoacoustic equation of motion. The method is very accurate and efficient and applies to situations where the relaxation times are far from the source frequency band. For instance, the seismic problem with relaxation times in the sonic band is a problem that the spectral Chebychev method cannot solve. Efficiency comparison with second-order time differencing reveals that the new approach is almost two times faster when two-digit precision is required. To obtain machine accuracy, very small time steps and, therefore, a large amount of CPU time are required with finite differencing, which makes it impractical for application to forward modeling algorithms. The present approach improves the situation by giving an accuracy within computer precision and not much additional CPU time. The last example involves calculation of a common-shot seismogram from a typical hydrocarbon trap. The model involves realistic material properties. A detailed description is given of how to handle this problem with the new technique. The results indicate the necessity of anelastic modeling for an appropriate interpretation of seismic data. The new technique will be very useful to solve the problem of wave propagation in a general anisotropic-viscoelastic medium where, due to the high number of calculations and required accuracy, an efficient algorithm is necessary.

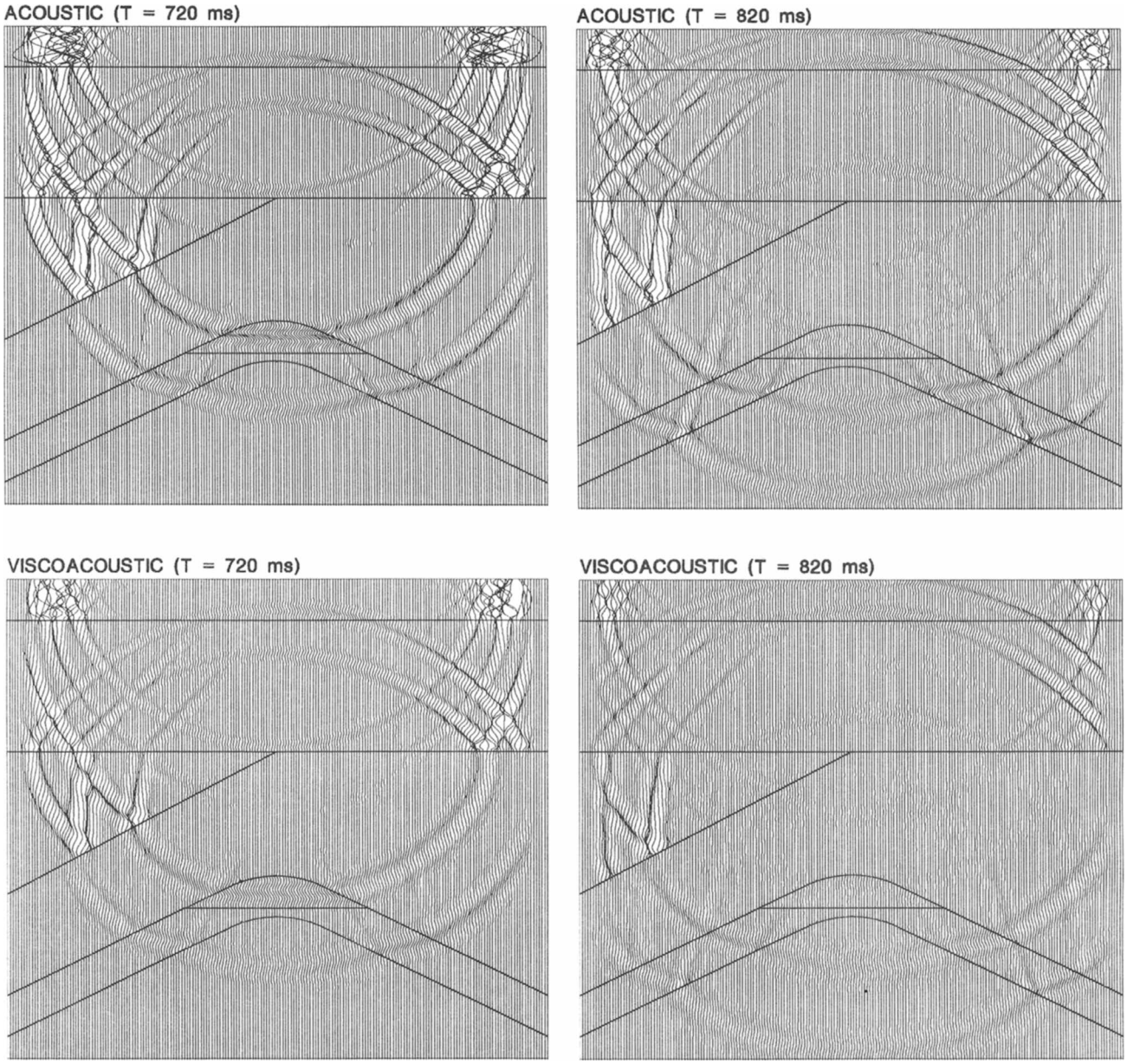

FIG. 8. Acoustic and viscoacoustic snapshots corresponding to the anticlinal trap model; (a) and (b) at 720 ms propagating time, and (c) and (d) at 820 ms propagating time.

ACKNOWLEDGMENTS

This work was supported by project EOS-1 (Exploration Oriented Seismic Modelling and Inversion), contract no. JOUF-0033, part of the JOULE Research and Development Programme (Section 3.1.1.6), of the Commission of the European Communities. We wish to thank Prof. A. Behle for useful comments on the original manuscript, and Dr. B. Kummer for helpful discussions on the anticlinal trap model. One of us (J.M.C.) has been aided by an Alexander von Humboldt scholarship.

REFERENCES

Borcherdt, R. D., 1982, Reflection-refraction of general *P* and type-I *S* waves in elastic and anelastic solids: Geophys. J. Roy. Astr. Soc., **70,** 621–638.

Carcione, J. M., Kosloff, D., and Kosloff, R., 1988a, Wave propagation simulation in a linear viscoacoustic medium: Geophys. J. Roy. Astr. Soc., **93,** 393–407.

———, 1988b, Wave propagation simulation in a linear viscoelastic medium: Geophys. J. Roy. Astr. Soc., **95,** 597–611.

———, 1988c, Viscoacoustic wave propagation simulation in the earth: Geophysics, **53,** 769–777.

Day, S. M., and Minster, J. B., 1984, Numerical simulation of attenuated wavefields using a Pade approximant method: Geophys. J. Roy. Astr. Soc., **78,** 105–118.

Emmerich, H., and Korn, M., 1987, Incorporation of attenuation into time-domain computations of seismic wave fields: Geophysics, **52,** 1252–1264.

Ferry, J. D., 1970, Viscoelastic properties of polymers: John Wiley & Sons, New York.

Hamming, R. W., 1973, Numerical methods for scientists and engineers: McGraw-Hill Book Co., Inc.

Kosloff, D., and Baysal, E., 1982, Forward modeling by a Fourier method: Geophysics, **47,** 1402–1412.

Kosloff, R., and Kosloff, D., 1986, Absorbing boundaries for wave propagation problems: J. Comp. Phys., **63,** 363–376.

Murphy, W. F., Winkler, K. W., and Kleinberg, R. L., 1986, Acoustic relaxation in sedimentary rocks: Dependence on grain contacts and fluid saturation: Geophysics, **51,** 757–766.

Szilard, J., 1982, Ultrasonic testing, non-conventional testing techniques: John Wiley & Sons, New York.

Tal-Ezer, H., 1985, Spectral methods in time for parabolic problems: ICASE rep. no. 85-9. NASA, Langley Research Center, Hampton, VA.

Tal-Ezer, H., 1989, Polynomial approximation of functions of matrices: J. Sc. Comp., **4,** 25–60.

Tal-Ezer, H., Kosloff, D., and Koren, Z., 1987, An accurate scheme for seismic forward modeling: Geophys. Prosp., **35,** 479–490.

Walsh, J. L., 1956, Interpolation and approximation by rational functions in the complex domain: Provid. R.I.

APPENDIX A

POLYNOMIAL APPROXIMATION OF THE EVOLUTION OPERATOR

Polynomial approximation of the evolution operator given in equation (14) can be reduced to approximating a function $f(z)$, analytic in a domain D which includes all the eigenvalues of $\mathbf{M}_N$, by polynomials (Tal-Ezer, 1989). In the homogeneous case:

$$f(z) = e^{tz}, \tag{A-1a}$$

and in the inhomogeneous case:

$$f(z) = \int_0^t e^{\tau z} h(t-\tau)\, d\tau, \tag{A-1b}$$

where we consider a separable source term of the form $\mathbf{S} = \mathbf{A}\mathbf{h}$, with $\mathbf{A}(\mathbf{x})$ the spatial distribution and $h(t)$ the time function. The domain D is given by

$$D=(z/z \in D_1 \cup D_2,\ D_1=[-A, 0];D_2 = [-iB, iB]), \quad A>0,\ B>0, \tag{A-2}$$

where

$$A \geq |\max\,[\lambda_v^{(1)}]|, \qquad B \geq \left|\lambda^{(2)}\frac{N}{2}\right|. \tag{A-3}$$

The approach is based on interpolation in the domain D, over a set of points known as Fejer points (Walsh, 1956). Getting these points is based on the following:

Let $\chi(u)$ be a conformal mapping from the u-plane to z-space, which maps the complement of a disc of radius δ to the complement of D, where δ is called the logarithmic capacity of D and is given by the limit $\delta = |\chi'(\infty)|$. The prime denotes derivative with respect to the argument. The analytic expression for $\chi(u)$ corresponding to the domain D is

$$\chi(u) = -\frac{B}{2}\left\{\left[\frac{1}{2}(1+E)\left(\frac{u}{\delta}+\frac{\delta}{u}\right)+1-E\right]^2-4\right\}^{1/2},$$

$$|u| = \delta, \tag{A-4}$$

where

$$E = \frac{\sqrt{A^2+B^2}}{B}, \qquad \delta = \frac{B(1+E)}{4}. \tag{A-5}$$

The same function $\chi(u\delta)$ maps the complement of the unit disc to the complement of the domain D. Then, Fejer points are

$$z_j = \chi(u_j), \qquad j = 0, \ldots, m-1, \tag{A-6}$$

where u_j are the m roots of the equation $u^m = \delta$, with m the degree of the polynomial. It is proven in Tal-Ezer (1989) that the set $[z_j]$, $j = 0, \ldots, m-1$ has maximal properties of convergence. Then, the sequence of polynomials $P_m(z)$ of degree m found by interpolation to an arbitrary function $f(z)$, analytic on D at the points z_j, converge maximally to $f(z)$ on D [see also the theorem in page 168 of Walsh (1956)]. The interpolating polynomial in Newton form is

$$P_m(z) = a_0 + a_1(z-z_0) + a_2(z-z_0)(z-z_1) + \cdots + a_m(z-z_0)\cdots(z-z_{m-1}), \tag{A-7}$$

where a_j is the divided difference of order j, (e.g., Hamming, 1973, p. 298),

$$a_j = f[z_0, \ldots, z_j], \qquad j = 0, \ldots, m-1. \tag{A-8}$$

Note that the time dependence is contained in these coefficients. When two interpolating points coincide (the case $z_j = z_{j+1}$, $j \leq m-1$ appears), the divided difference between these two points is calculated as

$$f[z_j, z_{j+1}] = \frac{df}{dz}(z_j), \tag{A-9}$$

with $f(z)$ given by equation (A-1a) or equation (A-1b).

When the logarithmic capacity δ is large, a_j will be very small. In this case, to avoid exceeding the dynamic range of the computer, it is convenient to work with $P_m(\delta\hat{z})$, where $\hat{z} = z/\delta$. The interpolating points and divided difference are normalized as

$$\hat{z} = z_j/\delta,$$

and

$$\hat{a}_j = \hat{f}[\hat{z}_0, \ldots, \hat{z}_j], \qquad j = 0, \ldots, m-1, \tag{A-10}$$

respectively, where $\hat{f}(\hat{z}) = f(z)$.

Computation of the interpolating points

This Fortran program shows how to arrange the interpolating points in order to get a high-degree interpolating polynomial insensitive to roundoff errors:

```
c       complex u(20),z(20),zz
c
c       Conformal mapping from the unit-circle (u-plane) to the
c       T-shape domain (z-plane).
c
        pi=3.14159265
        pi2=pi/2.
        m=20
        dtheta=2.*pi/m
c
c       Interpolating points in u-space
c
        u(1)=(1.,0.)
        u(2)=(-1.,0.)
        u(3)=(0.,1.)
        m1=(m+2)/2
        m2=m1/2-1
        do i=1,m2
        if(mod(m1,2).eq.0) then
        i1=2*i+1
        theta1=(m2-i+1)*dtheta
        theta2=pi-theta1
        else
        i1=2*(i+1)
        theta1=pi2-i*dtheta
        theta2=pi2+i*dtheta
        endif
        i2=i1+1
        u(i1)=exp((0.,1.)*theta1)
        u(i2)=exp((0.,1.)*theta2)
        end do
c
        A=700.
        B=350.
        E=sqrt(A*A+B*B)/B
c
c       Interpolating points in z-space
c
        z(1)=0.
        z(2)=-A
        do i=3,m,2
        zz=0.5*(1+E)*(u(i)+1./u(i))+(1.,0.)*(1-E)
        z(i)=-0.5*B*sqrt(zz**2-4)
        z(i+1)=conjg(z(i))
        end do
        stop
        end
```

APPENDIX B

PHASE VELOCITY DISPERSION IN THE SECOND-ORDER TIME-DIFFERENCING APPROXIMATION

Let us consider the 1-D viscoacoustic problem in a homogeneous medium. First, we evaluate the exact phase velocity dispersion. Let a plane-wave solution to equations (41a) and (41b) be of the form

$$e = e_0 e^{i(\omega t - k_c x)} \tag{B-1a}$$

and

$$e_{1\ell} = e_{1\ell 0} e^{i(\omega t - k_c x)} \tag{B-1b}$$

with k_c the complex wavenumber. Considering constant material properties, substitution of equations (B-1a) and (B-1b) into equations (41a) and (41b) gives

$$-\omega^2 e = -k_c^2\left[M_u e + \sum_{\ell=1}^{L} e_{1\ell}\right], \qquad \ell = 1, \ldots, L \quad \text{(B-2a)}$$

and

$$i\omega e_{1\ell} = e\phi_\ell - \frac{e_{1\ell}}{\tau_{\sigma\ell}}, \qquad \ell = 1, \ldots, L. \quad \text{(B-2b)}$$

Obtaining $e_{1\ell}$ from equation (B-2b) and replacing it in equation (B-2a) yields

$$\omega^2 e = k_c^2\left[M_u + \sum_{\ell=1}^{L} \frac{\tau_{\sigma\ell}\phi_\ell}{1 + i\omega\tau_{\sigma\ell}}\right] e. \quad \text{(B-3)}$$

Substituting in equation (B-3) M_u and ϕ_ℓ given by equations (42) and (11), respectively, the phase velocity is expressed as

$$c(\omega) = \frac{\omega}{\mathrm{Re}\,[k_c(\omega)]} = c_R\ \mathrm{Re}^{-1}\left\{\left[1 - L + \sum_{\ell=1}^{L} \frac{1+i\omega\tau_{\varepsilon\ell}}{1+i\omega\tau_{\sigma\ell}}\right]^{-1/2}\right\}, \quad \text{(B-4)}$$

where Re^{-1} means to take the real part and then invert the result. When $\omega \to 0$, $c(\omega) \to c_R$, the relaxed velocity, and when $\omega \to \infty$, $c(\omega) \to c_u$, the unrelaxed velocity given by

$$c_u = c_R\left[1 - \sum_{\ell=1}^{L}\left(1 - \frac{\tau_{\varepsilon\ell}}{\tau_{\sigma\ell}}\right)\right]^{-1/2}. \quad \text{(B-5)}$$

Because $\tau_{\varepsilon\ell} > \tau_{\sigma\ell}$, $\forall\ell$, then $c_u > c_R$.

Let us consider now the second-order approximation of the time derivatives in equations (41a) and (41b). Discretizing the time variable, equations (B-1a) and (B-1b) take the form:

$$e^q = e_0 e^{i(\omega q\Delta t - k_c x)}, \quad \text{(B-6a)}$$

and

$$e^q_{1\ell} = e_{1l0} e^{i(\omega q\Delta t - k_c x)}. \quad \text{(B-6b)}$$

A second-order Taylor approximation of the time derivatives implies

$$\ddot{e}^q = -\omega^2 s_\theta^2 e^q, \quad \text{(B-7a)}$$

and

$$\dot{e}^q_{1\ell} = i\omega s_\theta e^q_{1\ell}, \quad \text{(B-7b)}$$

where

$$s_\theta = \frac{\sin\theta}{\theta}, \qquad \theta = \frac{\omega\Delta t}{2}. \quad \text{(B-8)}$$

Following the same procedure to obtain the exact phase velocity, we get in this case

$$\hat{c}(\omega) = \frac{c_R}{s_\theta}\,\mathrm{Re}^{-1}\left\{\left[1 - L + \sum_{\ell=1}^{L} \frac{1 + i\omega\tau_{\varepsilon\ell}s_\theta}{1 + i\omega\tau_{\sigma\ell}s_\theta}\right]^{-1/2}\right\}. \quad \text{(B-9)}$$

When $\omega \to 0$, $\hat{c}(\omega) \to c_R$, and when $\omega \to \infty$, $\hat{c}(\omega) \to \infty$. In the acoustic limit ($\tau_{\varepsilon\ell} \to \tau_{\sigma\ell}$, $\ell = 1, \ldots, L$), we obtain the numerical phase velocity dispersion for an acoustic medium (Kosloff and Baysal, 1982):

$$\hat{c}(\omega) = \frac{c_R}{s_\theta}. \quad \text{(B-10)}$$

The stability criterion is given by the condition $\theta < 1$. Taking $\omega = c_u\kappa$, where κ is the real wavenumber, we get

$$c_u\Delta t < \frac{2}{\kappa}. \quad \text{(B-11)}$$

The largest κ is the Nyquist spatial frequency for which $\kappa = \pi/DX$. Then the stability criterion is defined by

$$c_u\frac{\Delta t}{DX} < \frac{2}{\pi}. \quad \text{(B-12)}$$

For accuracy, $\hat{c}(\omega)$ should not differ significantly from $c(\omega)$ in the source frequency band. Hence, comparing equations (B-4) and (B-9) implies that $s_\theta \simeq 1$, or equivalently $\theta \ll 1$. Then, it is required that $\Delta t \ll 1/\omega_0$, where ω_0 is the dominant frequency of the source. The error is greater in the viscoacoustic case than in the acoustic case, since the approximation (B-9) gives not only a different relaxed velocity (c_R/s_θ) but also different relaxation times ($\tau_{\varepsilon\ell}s_\theta$ and $\tau_{\sigma\ell}s_\theta$).